Journal of New Technology and Materials (JNTM)
J. New Technol. Mater.
Vol. 08, N°02 (2018)59-64

OEB Univ. Publish. Co.

The effect of sliding speed and normal load on the friction and wear behavior of TiO_2 thin films

Hafedh Dhiflaoui, Kaouther Khlifi and Ahmed Ben Cheikh Larbi

National High School of Engineers of Tunisia, University of Tunis, 5 Taha Hussein street, 1008 Tunis, Tunisia

Corresponding author: email: dhafedh@gmail.com

Received date: Jul. 07, 2017; revised date: Oct. 15, 2018; accepted date: Nov. 11, 2018

Abstract

The tribological behavior of TiO2 thin films was investigated against test parameters.The friction coefficient under different normal loads, sliding speeds, and numbers of cycles was studied using a micro-scratch tester.The surface morphology of the EPD layers was observed using atomic force microscopy (AFM), the composition of the EPD layer was determined from the peak intensity using an X-ray diffractometer (XRD) and mechanical properties of films was investigated by nanoindentation technique.The results showed that varying normal load or sliding speed influences the friction coefficient, the wear volume and the wear specific coefficient. It was found, also, that a change in the wear behavior occurs when a critical value of normal load is exceeded.

In fact, at low normal load (Fn< 1 N), the stable friction leads to an insignificant wear. Moreover, for Fn> 1 N, the friction decrease is induced by wear particles. The analysis developed in this paper confirms a good wear resistance of the TiO2 coatings.

Keywords: Electrophoretic Deposition, TiO2 thin films, Tribology, mechanical properties;

1. Introduction

Titanium oxide coatings are very important materials find numerous commercial applications such as self-cleaning glazing [1], water purification [2], sensors [3], photo-catalyst and photovoltaics [4], corrosion protective coatings [5] and coatings for biomedical applications [6].Photocatalytic coatings are most commonly and widely used approaches in protecting metallic substrates against deterioration. TiO2 is an important inorganic material because of its good physical properties, which make it appropriate for coating applications. Also, coatings of TiO2 were enhanced tribological properties of metal surfaces [7]. The positive influence of TiO2 oxide film on tribological properties of substrate material and the effect of process parameters on properties of TiO2 oxide film in the scientific literature was shown. R. Mechiakh et al. [8] indicated that XRD pattern of the TiO2 thin film exhibited an anatase peaks between 400 °C and 800 °C.When the calcination temperature was increased, TiO2 crystallize structure transformed from anatase to rutile. Rutile is a mineral composed predominantly of titanium dioxide (TiO2). Rutile, a common natural form of TiO2, is readily available, inexpensive and holds substantial wear resistance, mechanical and thermal properties [9].

In this study, TiO2 thin films were deposited on 316L stainless steel by electrophoretic deposition technique. These films were calcined at 850°C. The effects of calcination temperatures on the structure of TiO2 films were determined. The surface morphology and deposited TiO2 thin films on 316L were characterized with X-ray diffraction (XRD) and atomic force microscopy (AFM, model Nanoscope). Mechanical properties were evaluated using nano-indentation technique tester. The effect of normal load and the sliding speed on the tribological behavior of TiO2 coatings were determined by microscratch tester.

2. Experimental

2.1. Materials and Methods

In this study, Thin TiO2 films are deposited on 316L stainless steel substrates using the electrophoretic depositionEPD technique (figure 1). The electrolyte solution is composed of a mixture of 0.06 g of TiO2 nanopowder with 60 ml of absolute ethanol where ≥99.8%. An aluminum plate with a dimension of 20 X 15 mm2 was used as a counter electrode (anode).

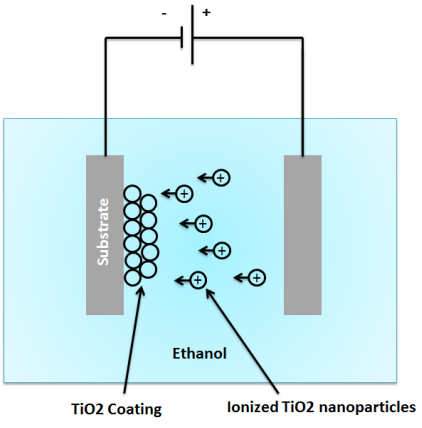

Figure 1. Electrophoretic deposition process

The suspensions were magnetically stirred for 5 min followed by 15 min ultra-sonification, subsequently followed by 5 min of stirring. The deposited layer on the substrate was heatedto 850°C for 2 h with a heating rate of 2.5°C/min in a furnace to evaporate any organic or volatile components. A desirable temperature due to the possible transformation of the anatase phase in the TiO2 particles will be converted to the rutile phase.

2.2. Testing Methods

2.2.1. Surface morphology

Atomic force microscopy (AFM) characterization, using model digital instrument-nanoscope (contact mode), was realized to examine the roughness of the anodizedsurfaces. Surface topography was recorded over scanned areas of 0.1 µm × 0.1 µm.

2.2.2. Mechanical properties

Mechanical properties of TiO2 films were investigated by nanoindentation experiments, using Nano Indenter NHT2 (CSM instruments, Suisse). The nanoindenter is equipped with a Berkovich diamond pyramid with a nominal angle of 65.3° and a nominal radius curvature of 20 nm radius at the tip of the indenter. The minimum allowed load is 0.1 mN, and the maximum load is 500 mN. Displacement recording resolution is 0.01 nm and the load recording resolution is 50 nN. Hardness and modulus are determined using stiffness calculated from the slope of the load–displacement curve during each unloading cycle.

2.2.3. X-ray diffraction analysis

The phase structure of the synthesized coatings was studied by X-ray diffraction technique where a Rigaku Multiflex instrument equipped with a Cu-Kα X-ray source (λ = 1.54178 °A) was used.

2.2.4. Friction test

Friction tests were carried out using a microscratch test (wear mode). Rockwell indenter of 0.05 mm radius, tangents the surface, it carries out a scratch at a constant normal load. The sensor system measures the normal and tangential forces in real time. For these tests, we can control the normal force (Fn), the sliding speed (V) and the sliding distance (L). Friction tests were carried out at a sliding speed (V) ranging from 100 to 300 µm/s under normal load (Fn) ranging from 1 to 5 N.

3. Results and discussion

3.1. X-ray Diffraction

Figure 2 shows X-ray diffractograms of the TiO2 coatings. The diffraction pattern of TiO2 coatings shows peaks of rutile phase located at 2θ = 27.4°, 36.1°, 39.2°, 54.3°, 62.7° and 69.03° corresponding to the (101), (101), (200), (211), (220) and (301) crystal faces, respectively. No peaks of anatase phase were detected. When temperature increased, the intensity of diffraction peaks of the anatase TiO2 became weaker at 750°C and disappears at 850°C. The grain size was calculated by using Debye-Scherer's formula from the full-width at half maximum (FWHM) of the (101) reflection [10,11]:

$$D = \frac{0{,}89.\lambda}{B.\cos\theta} \qquad (1)$$

Where D is the crystallite size or grain size, λ is the wavelength of X-ray, B is the full width at half maximum of diffraction peak and θ is the diffraction angle. The average grain size is about 71 nm.

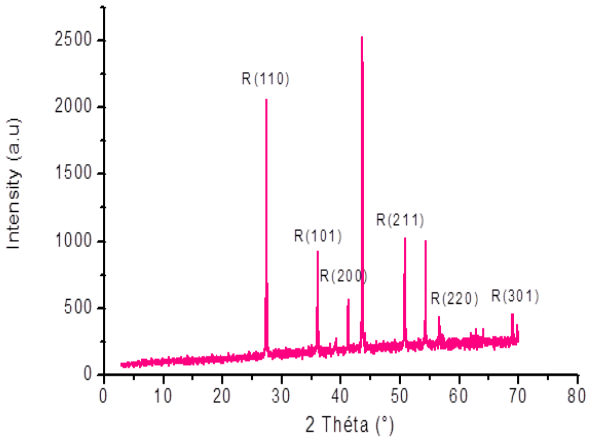

Figure 2. XRD patterns of the TiO2 coatings

3.2. AFM analysis

The surface morphology of TiO2 films was analyzed by atomic force microscopy (AFM, model Nanoscope).Micrographs were obtained in tapping mode under ambient conditions, using high resonance frequency

SiN cantilevers, with a pyramidal tip of 10 nm radius and a force constant of 0.032 N/m.

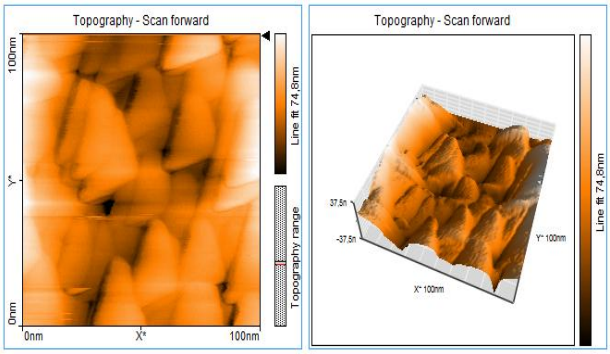

Figure 3. Three-dimensional AFM images

Figure 3 show typical three-dimensional representations (0.1 µm x 0.1 µm surface plots) of TiO2 coated sample. AFM revealed a rough surface texture consisted of particles fused together at the inter-particle contacts and deep valleys. Roughness Rms is about 50.3 nm.

3.3. Nanoindentation test

The nanoindentation tests were realized to measure the hardness and the Young's modulus of the coatings. A Berkovich diamond indenter was used to make indentations. The measurements of hardness and Young's modulus are mainly based on the unloading curve according to the Oliver and Pharr method [12].

The hardness is estimated from:

$$H = {}^{P}/_{A} \qquad (2)$$

Measurement of the elastic modulus follows from its relationship to contact area and the measured unloading stiffness through the relation:

$$\boldsymbol{S = \beta . \frac{2}{\sqrt{\pi}} . E_{eff} . \sqrt{A_c}} \qquad (3)$$

Where E_{eff} is the effective elastic modulus defined by:

$$\frac{1}{E_{eff}} = \frac{1-\vartheta^2}{E} + \frac{1-\vartheta_i^2}{E_i} \qquad (4)$$

The effective modulus takes into account the fact that elastic displacements occur in both the specimen, with Young's modulus E and Poisson's ratio ϑ, and the indenter, with elastic constants E_i and ϑi.

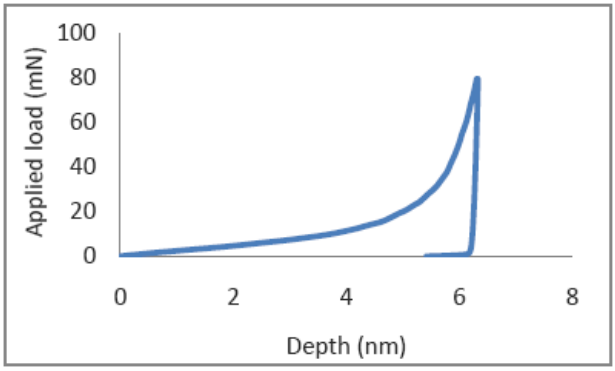

Figure 4. Load-displacement curve

Figure 4 shows a typical load-displacement curve of the TiO2 coating. The loading-unloading curve shows an initial increase in the penetration depth as a function of the load, and then plastic deformation occurs until the maximum load (Pmax = 80 mN), which relates to the maximum penetration depth (hmax = 5.4 nm). It is found that the hardness is about 88.57 MPa and Young's modulus is about 29.97 GPa.

4. Monotonous friction tests

4.1. Influence of the normal load (fn)

Monotonic friction tests were carried out at different normal loads (Fn = 1 N, Fn = 2 N and Fn = 5 N) Figure 5.

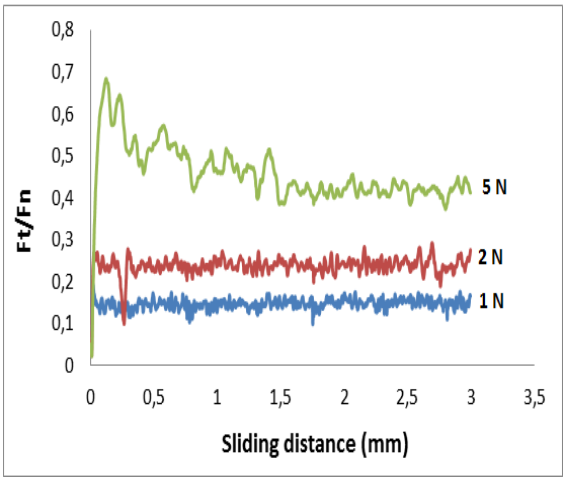

Figure 5. Influence of applied normal load of testing on friction with sliding distance at V = 100 µm/s.

The friction increases rapidly at the beginning of the test until reaching the full sliding contact (static friction) after which the friction coefficient reaches a constant value.

Table 1. Variation of average friction coefficient in relation to the normal load Fn (V = 100 µm/s)

Fn (N)	1	2	5
Dynamic friction coefficient (fd)	0.15	0.25	0.45

Figure 5 shows that under the same sliding speed, the friction coefficient increased with the load and the greater the load was, the longer the time would be from the beginning of stabilization.

- For low normal loads Fn ≤ 1 N, the friction coefficient is stable,
- For high normal loads Fn> 1 N, the friction coefficient presents a peak, which is normally attributed to full sliding condition (Ft = fFn), followed by a decrease until a stable value at the end of the friction test (fd = 0.45).

4.2. Influence of the friction speed

The friction tests were carried out at various sliding speeds V = 100, 200 and 300 µm/s. The evolution of the friction response in relation to the sliding speed (for Fn = 5 N and R = 0.05 mm) is illustrated by the curves in figure 6.

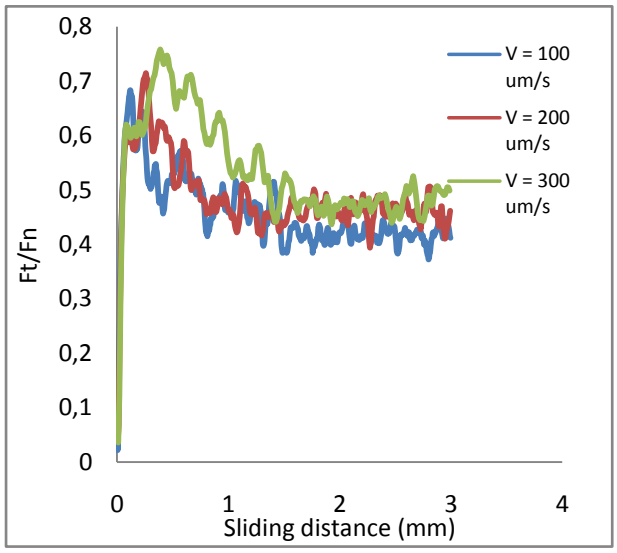

Figure 6. Influence of the friction speed of testing on friction with sliding distance under Fn = 5N.

The examination of this figure shows that the friction coefficient seems to increase with sliding speed.
An overview of wear tracks generated on tested samples is shown in Figure 7. For V = 300 µm/s, Figure shows the existence of surface polishing, micro-cracking, and detachment of wear particle. Micro-cracks were propagated outside the contact zone on both sides of the sliding direction following the frontward movement of the indenter.

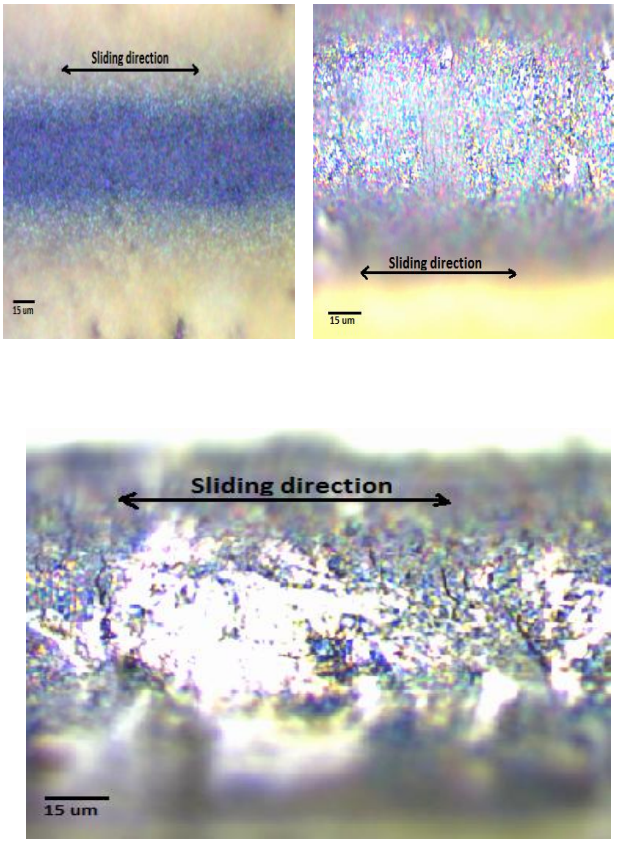

Figure 7. Optical images of the typical appearance of wear scarwith enlargement of x400, x800 and x4000

4.3. Cyclical friction tests

Figure 8 presents the variation of the dynamic friction coefficient on the sliding contact in terms of the number of cycles N (1 and 10 cycles) at an applied normal loads Fn = 1 N. The friction coefficient decreases in terms of the number of cycles. The friction coefficient decreases from 0.17 to 0.12 when the number of cycles increases. Inboth monotonous and cyclical cases, friction coefficient is more important when the normal load exceeds 1 N. Become necessary in order to study the correlation between frictions and wear mechanisms, in the next section.

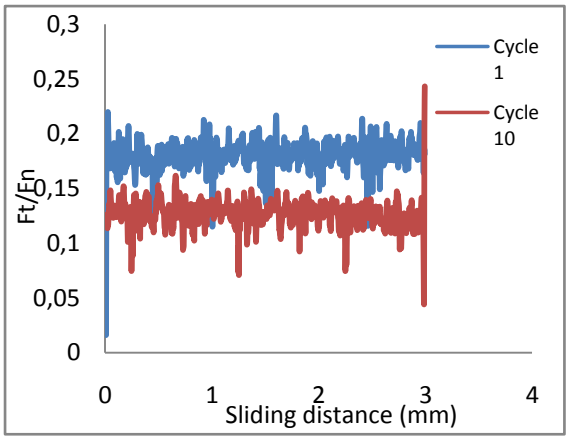

Figure 8. Influence of cycles numbers on friction with sliding distance at V = 100 µm/s.

5. Wear behavior

Wear coefficient is determined using Archard formula [13], equation (5):

$$K = \frac{V.HV}{F.L} \qquad (5)$$

V is the worn volume (mm3), F is the applied load (N), L is the sliding distance (mm), HV is the Vickers hardness and K is the Archard wear coefficient. The worn volume [14] is determined using equation (6):

$$V = \frac{l}{4}\left(D^2 \sin^{-1}\left(\frac{b}{D}\right) - b\sqrt{(D^2 - b^2)}\right) \qquad (6)$$

The worn volume is determined using mathematical approximations and experimental measures as worn track width 'b' (mm), worn track length 'l' (mm) and cylinder diameter 'D' (mm).

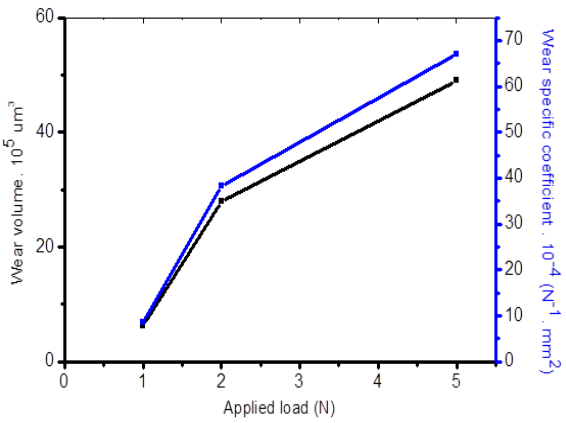

Figure 9. Variation of the wear specific coefficient and wear volume as function of applied load.

Figure 9 shows the variation of wear volume and the wear specific coefficient as function of applied load. Indeed, the wear volume obtained for an applied load of 1N is lower than which obtained with an applied load of 5 N. The change on wear kinetics occurs when curves of wear volume present a deviation in their direction. This phenomenon is, usually, shown when applied load exceeds 2 N. Das et al.[15] and Rai et al. [16] relate the wear rate variation to a critical value of load or velocity. Increasing normal load from 1 N to 5 N increases the wear coefficient. When normal load exceeds 2 N, wear coefficient behavior changes. This variation can be explained by the changes in the wear mechanisms at the interface under the effect of increasing of the contact pressure.

6. Conclusion

In this study, the effect of test conditions on the tribological properties was investigated. The results revealed that:

- Increasing the normal load decreases the friction coefficient but increases the wear volume and the wear coefficient.
- There is a critical normal load when it is exceeded the kinetics of wear changes.
- Increasing sliding speed decreases the friction coefficient
- The friction coefficient is more sensitive to the variation of normal load than sliding speed.

References

[1] A. Mills, G. Hill, S. Bhopal, I.P. Parkin, S.A. O'Neill,.A Chem.160 (3) (2003) 185–194.

[2] A. Fernandez, G. Lassaletta, V.M. Jimknez, A. Justo, Appl. Catal. B Environ. 7 (95) (1995) 49–63.

[3] O.K. Varghese, D. Gong, M. Paulose, K.G. Ong, C.A. Grimes, Sens. Actuators B Chem. 93 (1–3) (2003) 338–344.

[4] A. Fujishima, X. Zhang, D. Tryk, Surf. Sci. Rep. 63 (12) (2008) 515–582.

[5] A. R. Boccaccini, U. Schindler, H. Kruger, Mater. Lett. 51 (2001)225–230.

[6] S. Wu, Z. Weng, X. Liu, K.W.K. Yeung, P.K. Chu, Adv. Funct. Mater. 24 (35) (2014)5464–5481.

[7] D. Wang, Gordon.P. Bierwagen, Prog. Inorg. Coat. 64 (2009) 327–338.

[8] R. Mechiakh, N. Ben Sedrine, R. Chtourou, R. Bensaha, Appl. Surf. Sci. 257 (2010) 670–676.

[9] A. Rama, S. Kumar, S. Gurmel, O. P. Pandey Influence of particle size and temperature on the wear properties of rutile-reinforced aluminium metal matrix composite [J]. Journal of Composite Materials, 2014, doi: 10.1177/0021998314526079.

[10] B. D. Cullity, Elements of X-Ray Diffraction, 2nd ed.; Addison- Wesley: Reading, MA, 1978.

[11] P. Bilik, G. Plesch, Scr. Mater., 56 (2007) 979–982.

[12] W. Oliver, G. Pharr, J. Mater. Res. 19 (2004) 3–20.

[13] JF. Archard Contact and rubbing of flat surfaces. J Appl Phys 24 (1953)981–988.

[14] M.J. Perez M.M. Cisneros and H.F. Lopez Wear resistance of Cu–Ni–Mo austempered ductile iron. Wear, 260 (2006) 879–885.

[15] D. Das, A.K. Dutta and K.K. Ray, "Correlation of microstructure with wear behaviour of deep cryogenically treated AISI D2 steel", Wear; 267 (2009)1371–1380.

[16] D. Rai, B. Singh and J. Singh, "Characterisation of wear behaviour of different microstructures in Ni–Cr–Mo–V steel", Wear; 263 (2007) 821–829.